

Control of Micro- and Nanostructures of Layered Double Hydroxides by Hydrothermal Treatment

Keiichiro Maegawa, Fan Zhang, Qiaxian Johnson, Mihaela Jitianu, Wai Kian Tan, Go Kawamura, Atsunori Matsuda, and Andrei Jitianu*



Cite This: <https://doi.org/10.1021/acs.cgd.2c01124>



Read Online

ACCESS |



Metrics & More

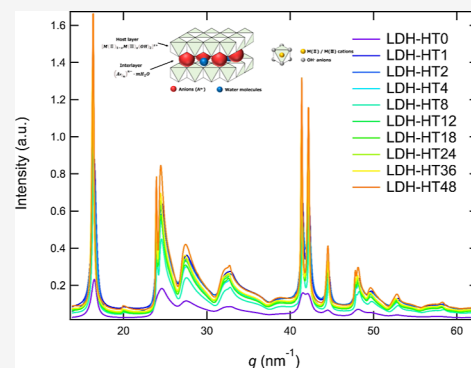


Article Recommendations



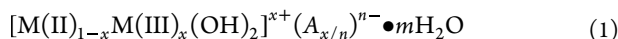
Supporting Information

ABSTRACT: Layered double hydroxides (LDHs) are mixed M(II) and M(III) hydroxides with positively charged lamellar brucite layers and interlayered anions. LDHs have attracted significant attention due to their anion- and cation-exchange ability, adsorption capacity, and potential applications in drug delivery and catalysis. The properties of LDHs directly correlate with their structures. In this study, we synthesized nickel-aluminum LDHs by the sol-gel method. We investigated the changes in their crystal structure/morphology introduced by hydrothermal treatments that varied from 0 to 48 h. Based on measured data using X-ray diffraction, scanning electron microscopy, transmission electron microscopy, and synchrotron-based small-angle X-ray scattering, we demonstrated that the duration of the hydrothermal treatment can effectively control the micro- and nanostructures of Ni–Al LDHs. We found that the hydrothermal treatment leads to a two-step change in the structure of the LDHs. In the first step, crystallization occurred during the first 24 h of hydrothermal treatment, increasing the interlayer width (from 2.28 to 2.31 nm) and the crystallite size (from 14.2 to 50.6 nm). In the second step, the predominant phenomena were stacking and planar expansion after the crystallization process approached equilibrium. Thus, the layered structure already developed in the first step was further stacked, and the hexagonal platelet characteristic of LDH expanded in a planar direction. Our study suggests that the duration of the hydrothermal treatment is a crucial factor in the structural evolution of LDHs and can be used to control the structure of LDHs for different applications.



1. INTRODUCTION

Layered double hydroxides (LDHs), also known as hydroxaltes, have been actively studied for several decades. A LDH exists in nature as a mineral and is classified as an anionic clay with the following general formula (eq 1) and structure (Figure 1).



Since Miyata reported the synthesis and physicochemical properties of LDHs,^{1,2} these compounds have been investigated for a broad range of applications such as drug delivery,^{3,4} water purification,^{5,6} catalysis for water splitting,^{7–9} and battery applications.^{5,10–12} LDHs have a multi-layer structure. The structure of each layer is similar to that of brucite ($[Mg(OH)_2]$), with the noticeable difference being that part of the divalent cations are replaced randomly by trivalent ones. This partial substitution of M(II) [e.g., Ni(II), Mg(II), Co(II), Cu(II), and Fe(II)] with M(III) [e.g., Al(III), Cr(III), Ga(III), Mn(III), and Fe(III)] leads to a positively charged brucite layer (cationic layer).^{1,2,13,14} Another layer exists between two cationic layers to compensate for this charge and maintain charge neutrality. This layer contains anions and water molecules and is commonly labeled as the interlayer. The chemical formula is given by eq 1, while

the structure is illustrated in Figure 1, where $[M(II)_{1-x}M(III)_x(OH)_2]^{x+}$ corresponds to the cationic brucite-type layer and $(A_{x/n})^{n-} \cdot mH_2O$ represents the anionic interlayer. For synthetic and natural LDHs, the most common anions in the interlayer are carbonate ions (CO_3^{2-}). However, various anions, such as NO_3^- , SO_4^{2-} , HO^- , PO_4^{3-} , and Cl^- , can be intercalated instead of carbonate ions in the interlayer using the ion-exchange method.^{15–17} The mixing ratio R , defined as $(1-x)/x$, where $1-x$ and x are the molar fractions of M(II) and M(III), respectively, characterizes the molar ratio between M(II) and M(III) ions present in the brucite-type layer. R determines the number of anions in the interlayer and can be directly correlated with the interlayer spacing. Subsequently, the interlayer spacing affects both electrochemical performance¹⁸ and the size of the LDH. The common mixing ratio R ranges between 2 and 4.^{19,20}

Received: October 4, 2022

Revised: February 14, 2023

Published: February 23, 2023

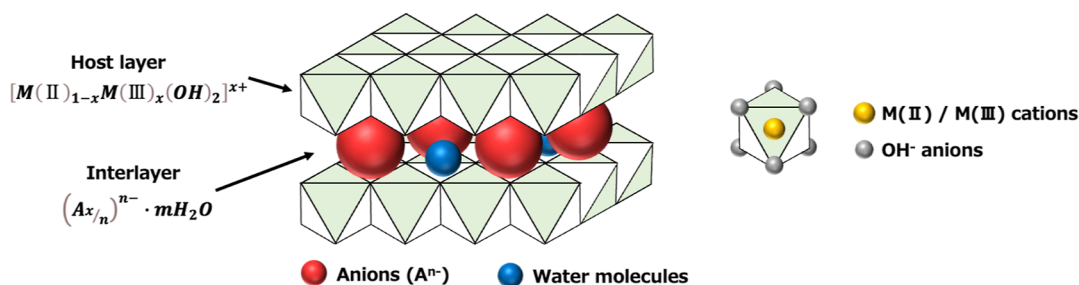


Figure 1. Schematics of the structure of LDHs.

Table 1. Structural Parameters of the Ni–Al LDH Samples as a Function of the Duration of Hydrothermal Treatment

sample	ratio (Ni ²⁺ /Al ³⁺)	HT time [hours]	lattice constant <i>c</i> (XRD) [nm]	crystallite size (XRD) [nm]	size of hexagonal plate-shape structure (SEM) [nm]	basal spacing (TEM) [nm]
LDH-HT0	3:1	0	2.28 (2)	8 (2)		
LDH-HT1	3:1	1	2.28 (2)	10 (2)		
LDH-HT2	3:1	2	2.28 (2)	9 (2)		
LDH-HT4	3:1	4	2.30 (2)	14 (3)	≈500	
LDH-HT8	3:1	8	2.27 (7)	17 (3)		
LDH-HT12	3:1	12	2.30 (1)	21 (4)		
LDH-HT18	3:1	18	2.31 (1)	24 (4)		
LDH-HT24	3:1	24	2.32 (2)	24 (4)	≈1500	≈0.759
LDH-HT36	3:1	36	2.32 (2)	25 (4)	≈1600	
LDH-HT48	3:1	48	2.31 (2)	27 (5)	≈2000	≈0.741

Predicting and tailoring LDH properties for targeted applications require a thorough understanding and control of the LDH structure. The structure influences the LDH's physical and chemical properties due to related changes in charge density and its distribution. Various studies have been performed to establish the structure–property relationships for LDHs.^{21–26} Traditionally, LDHs are prepared in the laboratory by precipitation at different pH values.^{23,27} As an alternative route of synthesis, Lopez et al.^{28–30} developed a sol–gel approach to prepare a Mg–Al LDH. Jitianu et al.³¹ also reported preparing Ni–Al LDHs with outstanding properties such as hydroxide ion conductivity and anion adsorption properties via a sol–gel method.^{19,21–24,32} Shivakumara et al. investigated the stacking disorder of LDHs by using a combined Rietveld analysis and DIFFaX simulation approach.³³ Hydrothermal treatment is a common approach to control and modify the LDH structure because it can reconstruct the LDH structure via anion intercalation.^{34,35} Kovanda et al.³⁶ reported the effect of hydrothermal treatment on thermal stability, pore sizes, and catalytic activity of Ni–Al LDHs synthesized through co-precipitation. However, the micro- and nanostructural transformation of sol–gel LDHs through hydrothermal treatment has received little attention. This is noteworthy because the platelet morphology of LDHs is expected to directly impact the physical/chemical properties of LDHs. This paper presents a systematic study of the impact of the duration of hydrothermal treatment on the structural transformation of LDHs. This work addresses the lack of these studies in the field and more importantly reveals how the length of the hydrothermal treatment affects the evolution of LDH crystallization and stacking and proposes possible mechanisms associated with the changes observed during this process.

In this study, we investigated the structural changes of LDH as a function of the duration of the hydrothermal treatment. We synthesized a Ni–Al LDH with the molar ratio of $R = 3$

using a sol–gel method. The as-synthesized LDH had low crystallinity with a secondary particle size in micrometers and a crystallite size in tens of nanometers. Since we noticed that different applications of LDHs require different nominal particle sizes,^{23,37} our goal for the hydrothermal treatment was to tailor the treatment duration for an ordered structure and desired particle size. Hydrothermal treatments were performed at 180 °C for different intervals of time (0, 1, 2, 4, 8, 12, 18, 24, 36, and 48 h). They were followed by analytical characterization using a suite of techniques, including X-ray diffraction (XRD), scanning electron microscopy (SEM), transmission electron microscopy (TEM), and synchrotron-based small-angle X-ray scattering (SAXS). Our results reveal the characteristics of physicochemical structural changes of LDHs by hydrothermal treatment and create opportunities to identify the optimal treatment time for LDHs in applications such as drug delivery, water purification, catalysis for water splitting, and batteries.

2. EXPERIMENTAL METHODS

2.1. Synthesis of LDH. We synthesized the Ni–Al LDH sample via a sol–gel method with the stoichiometric ratio between the M(II) and M(III) precursors as 3:1. We dissolved 3.72 g (18.2 mmol) of aluminum isopropoxide ($\text{Al}(\text{OCH}(\text{CH}_3)_2)_3$, 98+%) (Sigma-Aldrich¹) as the M(III) precursor in 100 mL of ethanol. 12 mL of hydrochloric acid (35.5% HCl) (Fisher Scientific) was added dropwise to peptize the precursor. Separately, 14.06 g (54.7 mmol) of nickel(II)2,4-pentanedionate ($\text{Ni}(\text{C}_5\text{H}_7\text{O}_2)_2$, 95–100%) (Gelest^a), as the M(II) precursor, was dissolved in 400 mL of ethanol. The two precursor solutions were admixed in a 1 L round-bottom flask with continuous stirring at 500 rotations per minute, under reflux conditions at 80 °C for 2 h. During the synthesis, the pH value of the reaction mixture would decrease as a gel was formed. Consequently, the pH of the solution was continuously adjusted and maintained constant at 8.5 using a total of 245 mL of 5% NaOH in ethanol solution during a week-long refluxing, while 75 mL of deionized water was added dropwise during this step to promote hydrolysis. After a week, the cooled reaction product was separated by filtration under vacuum,

followed by washing with deionized water. The product was dried at 110 °C for 24 h to remove ethanol and water. We washed the product to remove the impurities as follows: the filtered precipitate was redispersed in 200 mL of deionized water and stirred for 2 h, then filtered and dried at 110 °C. We repeated the washing process twice to obtain pure LDH. The resultant percentage yield was 64.5%.

2.2. Hydrothermal Treatment. We performed hydrothermal treatment (HT) at 180 °C for different durations in a 23 mL hydrothermal autoclave reactor (Parr) equipped with an inner polytetrafluoroethylene (PTFE) liner. For each HT, 0.3 g of the LDH sample, prepared as described above, was dispersed in 4.5 mL of deionized water. Sample details are presented in Table 1. In the sample identifier, the number following HT represents the duration of HT in hours.

2.3. Characterization. The phase analysis of LDH samples was performed using XRD (Rigaku, Ultima IV) equipped with a Cu anode. The X-ray wavelength was 0.15418 nm. The analysis was performed in a 2θ range of 5–80° with an angular resolution of 0.02°. The crystallite size was estimated using the Scherrer equation (eq 2),^{38,39} where D is the crystallite size in nm, θ is the diffraction angle in radians, K ($= 0.9$) is the Scherrer constant, λ is the X-ray wavelength, and β is the full width at half maximum (fwhm) in radians. The phase identification and lattice parameter analysis were performed using the PDXL (Rigaku) software. The simulated XRD patterns are provided in Figure S1.

$$D = K\lambda/\beta \cos \theta \quad (2)$$

An extensive-length-scale structural characterization of the LDH samples was performed using the ultra-small-angle X-ray scattering facility at the Advanced Photon Source, Argonne National Laboratory.⁴⁰ The instrument was used in its standard configuration, which, by combining scattering and diffraction measurements, probes a continuous size range from sub-Angstrom to several micrometers. The X-ray wavelength was 0.5904 Å. More details about this setup can be found elsewhere.⁴¹ All error bars indicated for the XRD/SAXS data represent the standard deviation. The error bar for the lattice constant c is the standard deviation value calculated by the PDXL software. As for the crystallite size, the error bar is attributed to the uncertainties. The approximately 15% error between the two crystallite size values calculated using the 003 and 006 diffraction lines by Scherrer's equation (eq 2) was used as the uncertainty.

The morphology of the LDH samples was evaluated using a HITACHI S-2700 scanning electron microscope. The SEM was operated at an acceleration voltage of 20 keV equipped with an AMT digital camera system. The LDH samples were mounted on aluminum stubs using carbon tape and then sputtered with gold prior to the analysis to reduce charging. High-resolution images of the LDH samples were acquired with a Hitachi HT7700 transmission electron microscope with a tungsten filament operating at 100 kV accelerating voltage. For TEM measurements, a small amount of each sample was dispersed in ethanol. A drop of the dispersion was deposited on a 300 mesh Formvar TEM grid (Ted Pella) and then dried in air overnight.

3. RESULTS

3.1. X-ray Diffraction Analysis. Figure 2a shows the XRD patterns for all samples. The peaks correspond to a hydroxyl-type phase (symmetry: $R\bar{3}m$) characteristic to LDH's crystal structure (ICDD: 01-089-0460).^{31,42–44} The XRD data of sample LDH-HT0 suggest that the as-synthesized material did not contain an appreciable amount of crystalline LDH compound.

Notably, we observed that the longer the HT duration, the sharper the XRD peaks, indicating that increasing HT time increases crystallinity. This is highlighted in Figure 2b, where the evolution of diffraction peaks characteristic to the 110, 113, and 116 peaks is shown. A rearrangement of the crystalline structure can explain the increase of crystallinity during the HT

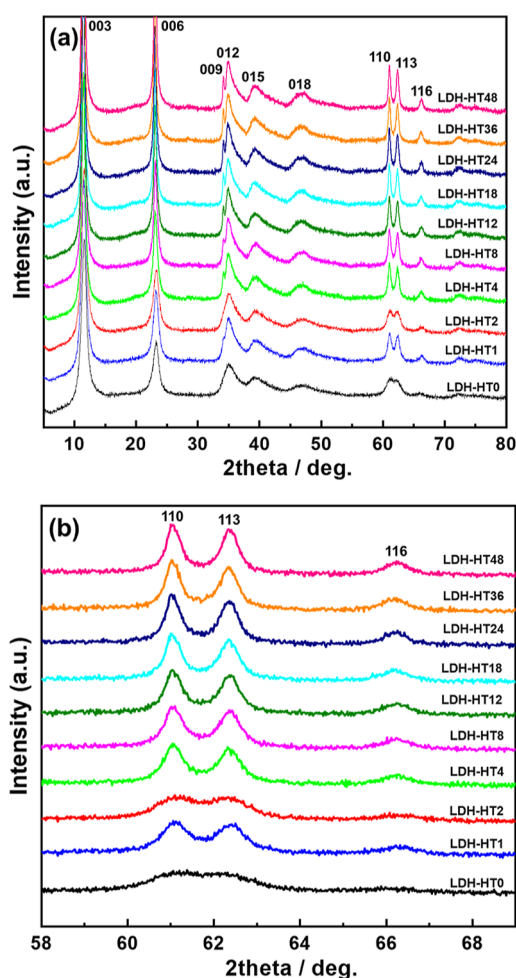


Figure 2. (a) XRD patterns of LDH samples hydrothermally treated for different intervals of time and (b) details of the diffraction pattern between 58 and 69° in 2θ , highlighting the sharpening of the XRD peaks with increasing hydrothermal treatment duration.

through a layered structure growth and delamination/reconstruction mechanism.²³

Based on the XRD data, we calculated the lattice constant c , and the results are shown in Table 1 and Figure 3. Specifically, the most intense peak near $2\theta = 11^\circ$ corresponds to the 003

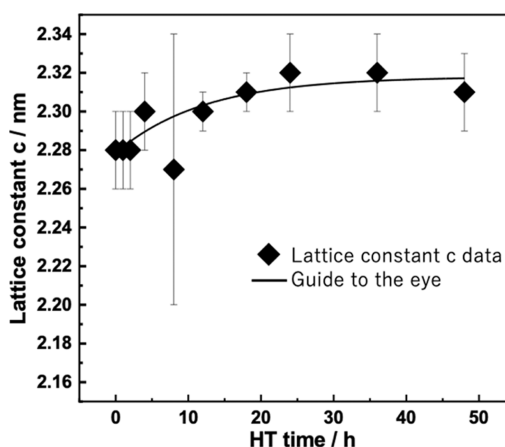


Figure 3. Lattice constant c (interlayer distance) as a function of time of hydrothermal treatment obtained by X-ray data.

reflections of LDH, enabling a straightforward calculation of the lattice constant c . The lattice constant c equals the total distance of the three cationic host layers and the three interlayers.⁴⁵ From Figure 3, the increasing of the duration of HT leads to an increase in the lattice constant parameter c . The change in lattice constant c can be mainly due to the change in the width of the interlayer. Our data suggest that the interlayer spacing increases rapidly during the first 24 h before reaching a plateau. The change in width can be explained by (1) decrease of chemical bonding energy between the host layer and the interlayer anions due to the changes in the charge density in the host layer or (2) mechanical expansion of the interlayer due to the increase in the number of water molecules and their arrangement in the interlayer.⁴⁶ According to our previous work, the interlayer anions are carbonate ions (CO_3^{2-}).³¹ The lattice parameters a and b remained relatively unchanged (Table S1).

We also estimated the crystallite size based on the Scherrer equation (eq 2) using the fwhm of the 003 peak (near $2\theta = 11^\circ$). The results, presented in Table 1 and Figure 4, clearly

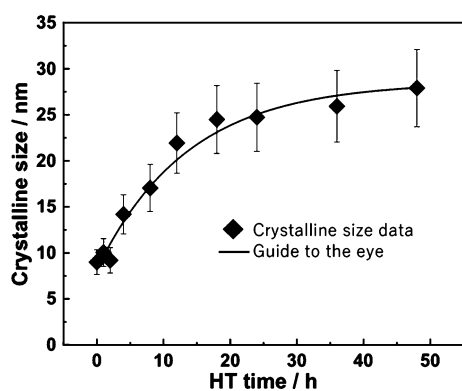


Figure 4. Variation of crystallite size as a function of time of hydrothermal treatment obtained by X-ray diffraction data.

demonstrate a growth of crystallite size with increasing HT duration. Interestingly, we observed that crystallite size continues to increase until approximately 18 h, and it remains constant after 24 h. This suggests that under the studied HT conditions, there might exist a thermodynamically stable crystallite size and its associated extent of structural reorganization, possibly due to the incorporation of interlayer anions.

3.2. SEM Observations. Figure 5 shows the evolution of LDH morphology after different periods of HT, as revealed by SEM. During the initial steps of HT (pristine and 2 h), slight morphological changes were detected. However, after 4 h of HT, the brucite hexagonal platelet-like microstructure, characteristic of hydrotalcites, emerged. Further HT led to growth of platelets, consistent with the previous reports.^{23,24,47}

These brucite hexagonal plate-shaped structures became increasingly visible under SEM after the HT duration exceeded 4 h. The typical HT-duration size dependence of the brucite platelet structures are summarized in Table 1. For example, the size of the brucite hexagonal plate-shaped structure is approximately 500 nm for the sample LDH-HT4 and increases with increasing HT duration. After 18 h, the LDHs appeared to consist of aggregates of the brucite plate-shaped structures primarily. We also observed an increase in the major dimension of the brucite plate-shaped structures, with the

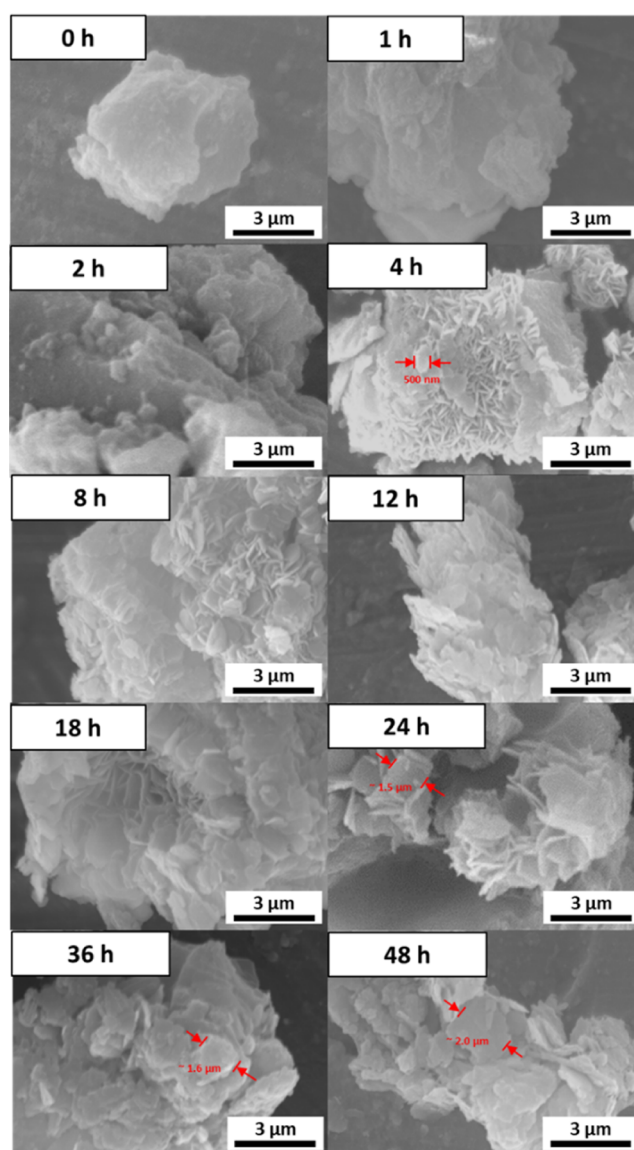


Figure 5. SEM micrographs of the LDH samples hydrothermally treated for different lengths of time.

dimension approaching $\approx 2 \mu\text{m}$ at 48 h. The sizes of the aggregates are on the order of several micrometers.

3.3. TEM Observations. Figures 6 and 7 show the TEM images of the studied samples. The TEM results indicate that the HT leads to two distinct phenomena (crystallization and growth of the brucite hexagonal platelets).

Owing to the TEM's spatial resolution, we observed the initial appearance of a small plate-shaped structure after a limited HT duration, such as those visible in the LDH-HT1 and LDH-HT2 data (Figure 6). For HT longer than 4 h, the brucite hexagonal platelets characteristic for the layered type structures of LDHs were evident, consistent with SEM observations. We also observed a monotonic growth of the platelets with increasing HT duration.

After 48 h of HT, the platelets expanded in the planer direction of the brucite-shaped structures. This phenomenon is more apparent in the high-resolution TEM images presented in Figure 7. These figures show that the LDH layered type structure becomes evident after a 4 h hydrothermal treatment (LDH-HT4). Consequently, after 48 h of hydrothermal

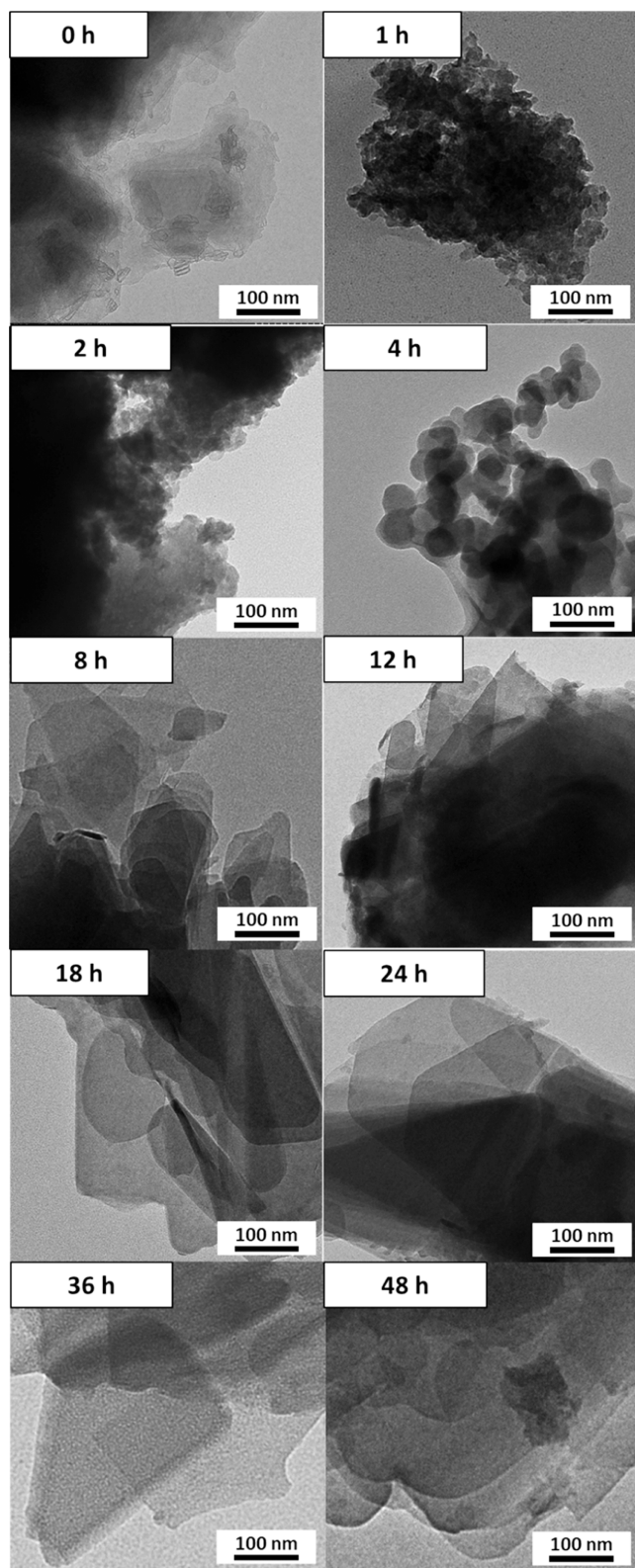


Figure 6. TEM micrographs of the LDH samples hydrothermally treated for different durations of time.

treatment (LDH-HT48), agglomerated large layered structures were observed. The growth of these structures is explained by the lamination/reconstruction mechanism determined by long-time hydrothermal treatment. By measuring the basal spacing ($c' = c/3$) of the lamellar structure observed by TEM (LDH-

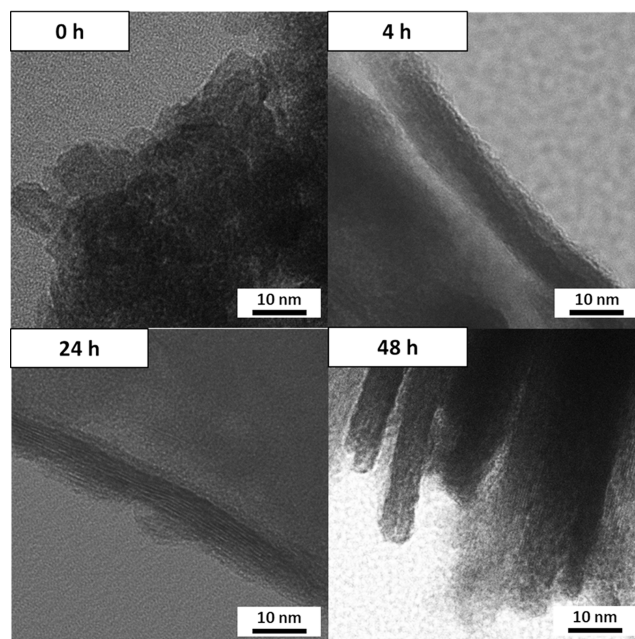


Figure 7. High-resolution TEM images of the samples hydrothermally treated for 0, 4, 24, and 48 h.

HT24 and LDH-HT48), the basal spacing for LDH-HT24 and LDH-HT48 was 0.759 and 0.741 nm, respectively (Table 1). As confirmed by TEM, there is no increase in the basal spacing between 24 and 48 h. The changes in the interlayer spacing were not observed, since these two samples have already crystallized. This result correlates with the lattice constant c parameters calculated by X-ray analysis exhibiting that the increase in the lattice constant c is saturated after a long HT duration as shown in Figure 3.

Here, the hexagonal platelet shape observed in SEM and TEM represents agglomeration of many crystallites which assemble in larger hexagonal platelets on the micro scale, contributing to the particle size. As a result, there is not a direct correlation between the values of the crystallite size derived by the Scherrer equation and the sizes observed in SEM/TEM.

3.4. SAXS. We performed combined SAXS/WAXS measurements to investigate the dependence of the structural and morphological properties of LDH on the HT duration. The SAXS data, plotted as a function of absolute scattering intensity as a function of the magnitude of scattering vector q , are summarized in Figure 8a. Here, $q = 4\pi \times \sin(\theta)/\lambda$, where θ is one-half of the scattering angle 2θ , and λ is the X-ray wavelength. Using the LDH-HT0 (Figure 8b) and LDH-HT48 h (Figure 8c) samples as examples, we can see that the SAXS profiles consist of two distinct components. The first component is a low- q power-law that does not have an associated Guinier region, suggesting the presence of a characteristic size beyond the instrument's detection limit ($\approx 6 \mu\text{m}$). This is typical for SAXS of powder samples.⁴⁸ Granular aggregates can readily form or individual powder size exceeds the instrumental limit, both observed in our materials, evidenced by SEM data. The second component consists of a Guinier region and its associated Porod region, as highlighted by the solid green lines in Figure 8b,c, respectively. The Guinier region reveals the presence of a characteristic size in the materials. In the case of LDH, the Guinier region shifts to the low- q region as the duration of HT increases, suggesting an

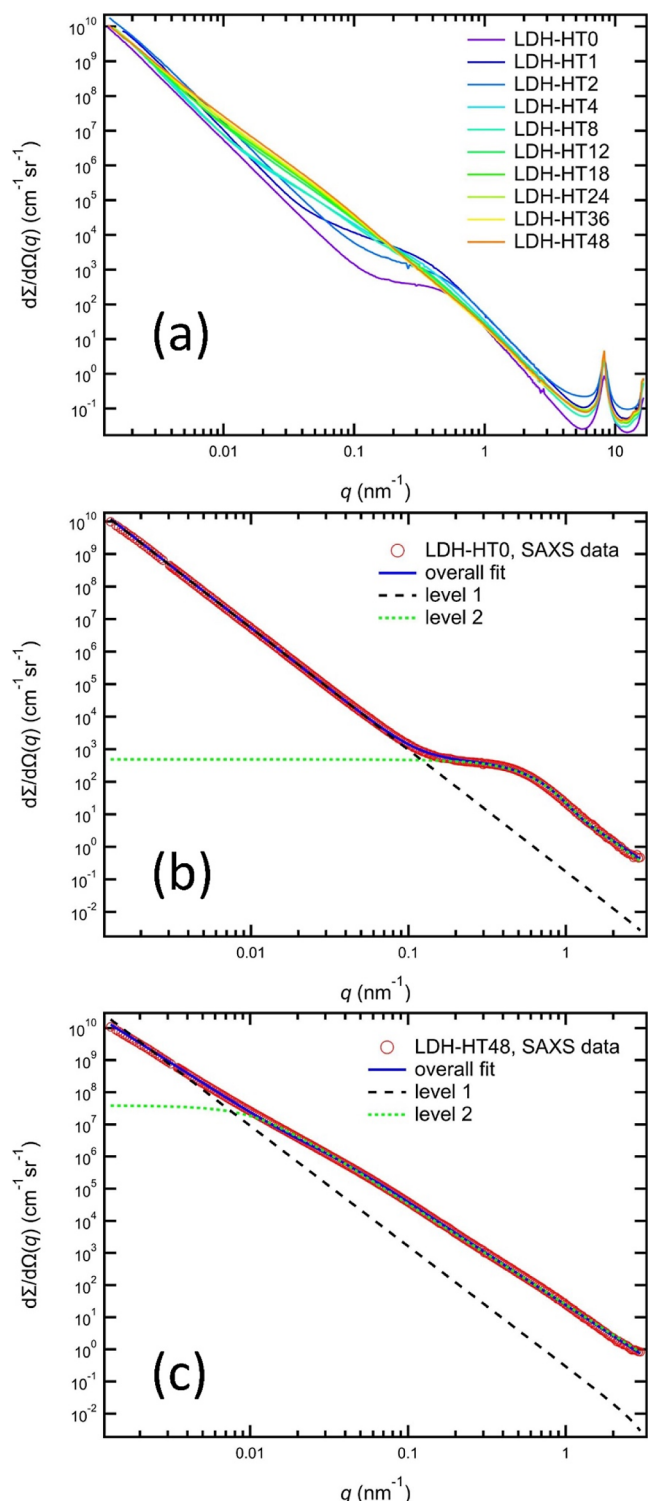


Figure 8. (a) Result of the SAXS analysis, (b) fitting model of LDH-HT0 as an example, and (c) fitting model of LDH-HT48 as an example.

increase in this characteristic size. In addition to these two SAXS components, the SAXS data also show a well-defined peak near $q = 0.08 \text{ nm}^{-1}$. This feature is related to the basal spacing of LDH and is the same as the 003 peak shown in Figure 2a.

We constructed a two-component model to describe the scattering profiles. Additional details about this type of

scattering model can be found elsewhere.^{49,50} This model describes the entire data set well. The characteristic size of the second component, as a function of the HT duration, is plotted in Figure 9. We observed a monotonic increase in this size with

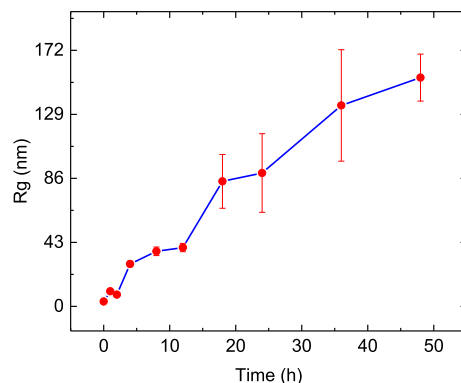


Figure 9. Variation of R_g as a function of hydrothermal treatment.

the increasing HT duration. This dimension exceeds both the interlayer spacing and the crystallite size. Qualitatively, it agrees with the observed size of platelets, not the brucite layer thickness as observed in TEM images in Figure 6. Because the SAXS dimensions are statistically averaged in contrast to TEM results where sampling is limited, we tentatively conclude that the LDH flakes underwent continuous coarsening along their small dimension during prolonged HT, where coarsening may be promoted by a dissolution and reprecipitation mechanism previously observed in Zn–Al LDHs.^{51,52}

Figure 10a shows WAXS (XRD) data of the LDH samples. Because these measurements were conducted in a transmission mode using a synchrotron instrument, both the sampling statistics and q resolution are superior to those of an in-house diffractometer. Nevertheless, both instruments' observed behaviors were consistent for the LDH samples. As HT duration increases, the crystallinity of LDH improves, as evidenced by narrower diffraction peaks. We also observed slight changes in peak positions, suggesting that HT leads to changes in atomic structures. In particular, based on the 003 peak near 0.08 nm^{-1} , we calculated the basal spacing (c'), which is 1/3 of the lattice constant c of LDH. As with the lattice constant c , the leading cause of the change in c' can be attributed to the incorporation of anions in the interlayer. The basal spacing's dependence on the HT duration is shown in Figure 10b. We observed a rapid increase in this distance during the initial period of HT. This distance reaches a plateau after approximately 18 h of HT. We used an exponential decay function to fit the time dependence of the basal spacing empirically. We found that it describes the process well, as demonstrated by the solid line in Figure 10b.

4. DISCUSSION

We systematically investigated the structure and morphology evolution of the Ni–Al sol–gel LDH under hydrothermal treatment for up to 48 h. The XRD results suggest that the pristine LDH synthesized by the sol–gel method contains a limited long-range order and is partially amorphous. By increasing the duration of the HT, the atomic ordering of LDH improved through a layered structure growth and delamination/reconstruction mechanism, resulting in a highly crystalline structure.⁴²

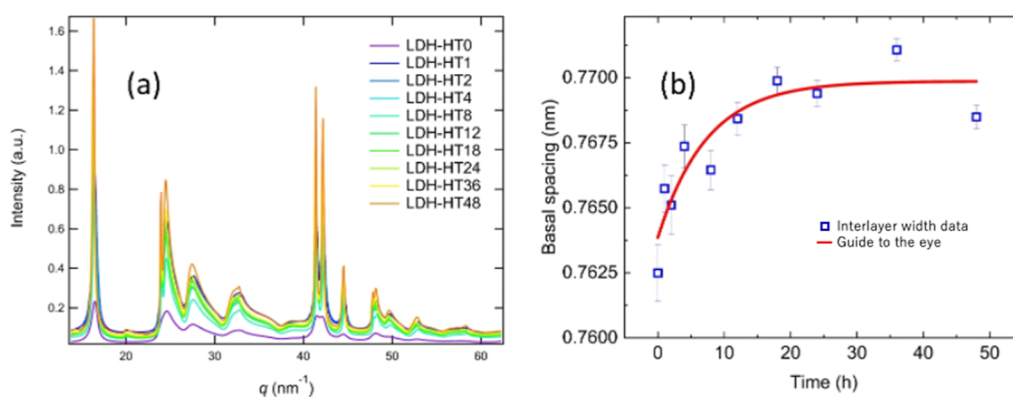


Figure 10. (a) XRD results obtained in the high-angle side of SAXS analysis and (b) basal spacing c' ($= c/3$) obtained by SAXS data as a function of time of hydrothermal treatment.

Initially, between 12 and 24 h, an improvement of the atomic ordering of LDH occurred by HT. This improvement of the atomic order was identified and corroborated by XRD, SEM, and TEM analyses. The first qualitative information was obtained by analyzing the diffraction lines of the XRD patterns, which became sharper, showing that LDH crystallizes with the increasing time of HT. Quantitatively, the evolution of the lattice parameter c and the crystallite size illustrated in Figures 3 and 4 demonstrate a similar dependence with the duration of the HT treatment. The characteristics of the lattice parameter c and the crystal size are proof of the increase in the crystallinity. It was observed that the lattice parameter c and the crystal size increased up to 18 h and stopped growing after 24 h. These results suggest that a thermodynamically stable interlayer distance and crystal size exist for this type of LDH. Incorporating anions that lead to the increase of interlayer distance also contributes to the increase in crystallite size. The SEM data (Figure 5) closely corroborate with the X-ray analysis results showing that the LDH before hydrothermal treatment (LDH-HT0) presents a disordered structure without well-organized layers. After 4 h of HT, the brucite-type layers start to develop the characteristic LDH hexagonal shape, indicating the progress of crystallization. This trend follows with a continuous and gradual formation of LDH crystallites until 24 h of HT. After 24 h, no significant changes in the LDH structures were observed, except an increase in the planar growth of the brucite platelets. This trend for the samples to behave differently after a hydrothermal treatment time of approximately 24 h is in good agreement with the XRD data. The crystallite size evolution shown in Figure 4 reveals a similar trend with the c parameter presented in Figure 3. Hence, it can be considered that the hydrothermal treatment of LDH leads to crystallization through the increase of the interlayer thickness and crystallite growth up to about 24 h. The TEM results (Figures 6 and 7) also support the above discussion. In the first 24 h, the amorphous structure observed for the pristine LDH sample (0 h) was rearranged and began to show a typical brucite hexagonal platelet-like shape for the samples that had undergone HT for more than 4 h. The TEM images (Figure 7) clearly showed a characteristic lamellar pattern of the layered structure of LDH for the samples hydrothermally treated for at least 4 h. The appearance of this lamellar pattern is probably related to the increase of crystallinity and crystallite size. Crystallization regularizes the atomic arrangement, leading to an increase in the interlayer spacing (Figure 3) and an increase in the crystallite size

(Figure 4), making the layered structure visible. It can be concluded that this process of crystallization by hydrothermal treatment is expected to be approaching equilibrium at about 24 h.

The change in the structure of LDH by hydrothermal treatment does not end at 24 h. Although the changes in the crystallographic parameter, such as lattice parameter c (Figure 3) and crystallite size (Figure 4) were almost not observed after 24 h. However, morphological changes were observed in SEM, TEM, and SAXS. Then after crystallization was finalized, the evolution of the LDH sample toward an agglomeration process became apparent, as displayed in the SEM images (Figure 5). This agglomeration process was more clearly confirmed in the TEM analysis. After 24 h, planar growth occurred; the crystallized structure, which was completed at about 24 h, started to be further spread out in the planar direction (Figure 6). Furthermore, during this step, besides the planar growth of the crystallized structure, lamination and stacking of the layered structure was illustrated only by the TEM analysis and not observed in the SEM analysis (Figure 5). This was achieved through the mechanism of delamination and reconstruction via hydrothermal treatment.^{35,53}

SAXS measurements provided additional insights that are consistent with the discussions above. The presence of a characteristic size that is beyond the detection limit of the instrument ($\approx 6 \mu\text{m}$) was confirmed (Figure 8b,c). This result correlates with the results of the SEM image. The agglomerated particles a few micrometers in size identified in the SEM image are particles with a size exceeding the SAXS system's resolution. According to the result of R_g (radius of gyration) in Figure 9, monotonic increase was seen in the characteristic size with increasing HT duration. From this result, this characteristic size as R_g is not correlated with the crystalline size and the interlayer size due to the different phenomena illustrated in Figures 3 and 4. Instead, the increase in R_g may be attributed to the spreading/lamination of the layered structure as confirmed by TEM. As can be seen from the TEM image in Figure 6, the growth of a single hexagonal plate is called spreading, and the stacking of the plates, seen in the enlarged image in Figure 7, is called lamination. The width of the brucite hexagonal platelets or the cross-sectional heights of the stacked LDH layers in the TEM images (Figures 6 and 7) can be roughly correlated with the R_g values (Figure 9). Figure 10 follows the XRD data shown in Figure 2 and Figure 3. Figure 10b, the basal spacing c' ($= c/3$) shows a similar characteristic with the lattice parameter c obtained by XRD

analysis. Using a simple exponential decay model, we identified a characteristic time scale of (7.3 ± 4.1) h for the evolution of this interlayer spacing. These results also support our hypothesis that structural changes of LDH by HT have two phases.

To summarize the discussion so far, the structural change of LDH by HT occurs in two steps. Crystallization of the LDH structure has mainly occurred during 24 h of HT. During this first step, crystallization and growth of the interlayer thickness along with an increase in crystallite size were observed. After 24 h, the second step begins and is illustrated by the planar growth of the structure. After the LDH layered structure was established by crystallization, it started to laminate and expanded in the planar direction. These stacking and expanding trends are correlated with increasing of the Rg. It is possible to control the structure of LDH by controlling the duration of the hydrothermal treatment. Since crystallization is saturated after 24 h, a hydrothermal treatment time of 24 h is the optimum time to obtain a highly crystalline LDH. If the hydrothermal treatment is carried out for longer, the degree of crystallization does not increase any further and the main effect is to increase the size of the LDH plates. In summary, it was found that it is possible to control the structure of LDH as desired, depending on the intended application and the specific properties associated with it.

5. CONCLUSIONS

In summary, changes in the crystal, interlayer spacing and morphological structure of the Ni–Al-type LDH by the hydrothermal treatment were studied and evaluated using XRD, SEM, TEM, and SAXS. The LDH synthesized via the sol–gel method showed a partially amorphous-like structure. The hydrothermal treatment increased this crystallization. Our experimental evidence shows two steps of structural changing of the LDH during the hydrothermal treatment, crystallization followed by lamination/expansion. The first step, crystallization, occurred in the first 4–24 h of the hydrothermal treatment when the interlayer width expanded and the crystallite size grew. The arranged layered structure was laminated and expanded in the planar direction during the second step. According to these results, we can conclude that the structure of the LDH can be managed by controlling the time of the hydrothermal treatment. The crystallization process is saturated after 24 h, so a hydrothermal treatment time of 24 h is optimal if the aim is to obtain a LDH with high crystallinity. If the hydrothermal treatment is extended beyond 24 h, although the crystallinity will not increase any further, the main effect will be increasing the size of the LDH plates. Differences in crystal structures and morphologies influence the LDH properties, making them suitable for different applications. This study was able to provide essential insights into the change in the crystallization and morphology during the hydrothermal treatment, which can be further used to tailor LDH structural characteristics for targeted applications.

■ ASSOCIATED CONTENT

SI Supporting Information

The Supporting Information is available free of charge at <https://pubs.acs.org/doi/10.1021/acs.cgd.2c01124>.

Simulated XRD patterns of prepared Ni–Al LDHs as a function of the duration of hydrothermal treatment and structural parameters of the Ni–Al LDH samples

obtained by the XRD analysis as a function of the duration of hydrothermal treatment (PDF)

■ AUTHOR INFORMATION

Corresponding Author

Andrei Jitianu – Department of Chemistry, Lehman College, CUNY, West Bronx, New York 10468, United States; Ph.D. Program in Chemistry and Biochemistry, The Graduate Center of the City University of New York, New York, New York 10016, United States; orcid.org/0000-0001-6111-531X; Email: ANDREI.JITIANU@lehman.cuny.edu

Authors

Keiichiro Maegawa – Department of Chemistry, Lehman College, CUNY, West Bronx, New York 10468, United States; Department of Electrical and Electronic Information Engineering, Toyohashi University of Technology, Toyohashi, Aichi 441-8580, Japan

Fan Zhang – Materials Measurement Science Division, National Institute of Standards and Technology, Gaithersburg, Maryland 20899-8520, United States; orcid.org/0000-0003-1248-0278

Qiaxian Johnson – Department of Chemistry, William Paterson University, Wayne, New Jersey 07470, United States

Mihaela Jitianu – Department of Chemistry, William Paterson University, Wayne, New Jersey 07470, United States

Wai Kian Tan – Institute of Liberal Arts and Science, Toyohashi University of Technology, Toyohashi, Aichi 441-8580, Japan; orcid.org/0000-0002-0014-5475

Go Kawamura – Department of Electrical and Electronic Information Engineering, Toyohashi University of Technology, Toyohashi, Aichi 441-8580, Japan; orcid.org/0000-0001-6585-7636

Atsunori Matsuda – Department of Electrical and Electronic Information Engineering, Toyohashi University of Technology, Toyohashi, Aichi 441-8580, Japan; orcid.org/0000-0002-6493-1205

Complete contact information is available at: <https://pubs.acs.org/10.1021/acs.cgd.2c01124>

Author Contributions

K.M. took the lead in synthesis, analysis, data processing, and writing the paper on this work. F.Z. conducted the SAXS measurement and analysis and supported the construction of the argument underlying this paper. Q.J. obtained all TEM images in this paper. M.J. advised the synthesis and characterization method of LDHs and was part of useful discussion. T.W.K. discussed the experimental methods and data analysis methods. G.K. helped the discussion of the obtained data. A.M. supervised the synthesis/analysis methods of LDHs. A. J. provided comprehensive support from acquiring research funding to establish the research concept, experimentation, discussion, and writing. All authors provided comments on the paper. All authors have seen and approved the paper, which has not been accepted or published elsewhere.

Notes

The authors declare no competing financial interest.

■ ACKNOWLEDGMENTS

Use of the Advanced Photon Source, an Office of Science User Facility operated for the U.S. Department of Energy (DOE)

Office of Science by Argonne National Laboratory, was supported by the U.S. DOE under contract no. DE-AC02-06CH11357.

ADDITIONAL NOTE

^aThe full description of the procedures used in this paper requires the identification of certain commercial products and their suppliers. The inclusion of such information should in no way be construed as indicating that such products or suppliers are endorsed by NIST or are recommended by NIST or that they are necessarily the best materials, instruments, software, or suppliers for the purposes described.

REFERENCES

- (1) Miyata, S. The Syntheses of Hydrotalcite-Like Compounds and Their Structures and Physico-Chemical Properties I: The Systems $Mg^{2+}\cdot Al^{3+}\cdot NO_3^-$, $Mg^{2+}\cdot Al^{3+}\cdot Cl^-$, $Mg^{2+}\cdot Al^{3+}\cdot ClO_4^-$, $Ni^{2+}\cdot Al^{3+}\cdot Cl^-$ and $Zn^{2+}\cdot Al^{3+}\cdot Cl^-$. *Crays Cray Miner.* **1975**, *23*, 369–375.
- (2) Miyata, S. Anion-Exchange Properties of Hydrotalcite-Like Compounds. *Clays Clay Miner.* **1983**, *31*, 305–311.
- (3) Fahami, A.; Beall, G. W. Structural and morphological characterization of $Mg_{0.8}Al_{0.2}(OH)_2Cl^{0.2}$ hydrotalcite produced by mechanochemistry method. *J. Solid State Chem.* **2016**, *233*, 422–427.
- (4) Bi, X.; Zhang, H.; Dou, L. Layered double hydroxide-based nanocarriers for drug delivery. *Pharmaceutics* **2014**, *6*, 298–332.
- (5) Daud, M.; Kamal, M. S.; Shehzad, F.; Al-Harathi, M. A. Graphene/layered double hydroxides nanocomposites: A review of recent progress in synthesis and applications. *Carbon N. Y.* **2016**, *104*, 241–252.
- (6) Zubair, M.; Daud, M.; McKay, G.; Shehzad, F.; Al-Harathi, M. A. Recent progress in layered double hydroxides (LDH)-containing hybrids as adsorbents for water remediation. *Appl. Clay Sci.* **2017**, *143*, 279–292.
- (7) Zhang, C.; et al. Layer-by-layer assembly of exfoliated layered double hydroxide nanosheets for enhanced electrochemical oxidation of water. *J. Mater. Chem. A* **2016**, *4*, 11516–11523.
- (8) Anantharaj, S.; Karthick, K.; Kundu, S. Evolution of layered double hydroxides (LDH) as high performance water oxidation electrocatalysts: A review with insights on structure, activity and mechanism. *Mater. Today Energy* **2017**, *6*, 1–26.
- (9) Fan, K.; et al. Nickel-Vanadium monolayer double hydroxide for efficient electrochemical water oxidation. *Nat. Commun.* **2016**, *7*, 1–9.
- (10) Long, X.; Wang, Z.; Xiao, S.; An, Y.; Yang, S. Transition metal based layered double hydroxides tailored for energy conversion and storage. *Mater. Today* **2016**, *19*, 213–226.
- (11) Kubo, D.; Tadanaga, K.; Hayashi, A.; Tatsumisago, M. Hydroxide ion conduction in Ni-Al layered double hydroxide. *J. Electroanal. Chem.* **2012**, *671*, 102–105.
- (12) Kubo, D.; Tadanaga, K.; Hayashi, A.; Tatsumisago, M. Multifunctional inorganic electrode materials for high-performance rechargeable metal-air batteries. *J. Mater. Chem. A* **2013**, *1*, 6804–6809.
- (13) Hou, X.; Bish, D. L.; Wang, S. L.; Johnston, C. T.; Kirkpatrick, R. J. Hydration, expansion, structure, and dynamics of layered double hydroxides. *Am. Mineral.* **2003**, *88*, 167–179.
- (14) He, J.; et al. Preparation of layered double hydroxides. *Struct. Bond* **2006**, *119*, 89–119.
- (15) Furukawa, Y.; Tadanaga, K.; Hayashi, A.; Tatsumisago, M. Evaluation of ionic conductivity for Mg-Al Layered Double Hydroxide intercalated with inorganic anions. *Solid State Ionics* **2011**, *192*, 185–187.
- (16) Kubo, D.; et al. Enhanced hydroxide ion conductivity of Mg-Al layered double hydroxide at low humidity by intercalating dodecyl sulfate anion. *J. Ceram. Soc. Jpn.* **2019**, *127*, 788–792.
- (17) Narita, E. Intercalation property of layered double hydroxides and its applications. *Nendo Kagaku* **2007**, *46*, 207–218.
- (18) Tan, Z.; et al. In Situ Formation of NiAl-Layered Double Hydroxide with a Tunable Interlayer Spacing in a Confined Impinging Jet Microreactor. *Energy and Fuels* **2020**, *34*, 8939–8946.
- (19) Iyi, N.; Sasaki, T. Deintercalation of carbonate ions and anion exchange of an Al-rich MgAl-LDH (layered double hydroxide). *Appl. Clay Sci.* **2008**, *42*, 246–251.
- (20) Tadanaga, K.; Furukawa, Y.; Hayashi, A.; Tatsumisago, M. Effect of Mg/Al Ratio on Hydroxide Ion Conductivity for Mg-Al Layered Double Hydroxide and Application to Direct Ethanol Fuel Cells. *J. Electrochem. Soc.* **2012**, *159*, B368.
- (21) Yang, H.; Chen, Z.; Guo, P.; Fei, B.; Wu, R. B-doping-induced amorphization of LDH for large-current-density hydrogen evolution reaction. *Appl. Catal. B Environ.* **2020**, *261*, 118240.
- (22) Yu, L.; et al. Amorphous NiFe layered double hydroxide nanosheets decorated on 3D nickel phosphide nanoarrays: a hierarchical core-shell electrocatalyst for efficient oxygen evolution. *J. Mater. Chem. A* **2018**, *6*, 13619–13623.
- (23) Zhang, P.; Yamaguchi, T.; Nair, B. N.; Miyajima, K.; Anilkumar, G. M. Mg-Al layered double hydroxides: A correlation between synthesis-structure and ionic conductivity. *RSC Adv.* **2014**, *4*, 41051–41058.
- (24) Hibino, T. Layered double hydroxide-agarose composites for water treatment: Carbonate contamination during the drying process. *Appl. Clay Sci.* **2015**, *116–117*, 93–101.
- (25) Sun, P.; et al. Single-layer nanosheets with exceptionally high and anisotropic hydroxyl ion conductivity. *Sci. Adv.* **2017**, *3*, e1602629–e1602636.
- (26) Long, J.; Yang, Z.; Huang, J.; Zeng, X. Self-assembly of exfoliated layered double hydroxide and graphene nanosheets for electrochemical energy storage in zinc/nickel secondary batteries. *J. Power Sources* **2017**, *359*, 111–118.
- (27) Saha, S.; Ray, S.; Ghosh, S.; Chakraborty, J. pH-dependent facile synthesis of CaAl-layered double hydroxides and its effect on the growth inhibition of cancer cells. *J. Am. Ceram. Soc.* **2018**, *101*, 3924–3935.
- (28) Lopez, T.; Ramos, E.; Bosch, P.; Asomoza, M.; Gomez, R. DTA and TGA characterization of sol-gel hydrotalcites. *Mater. Lett.* **1997**, *30*, 279–282.
- (29) López, T.; Bosch, P.; Asomoza, M.; Gómez, R.; Ramos, E. DTA-TGA and FTIR spectroscopies of sol-gel hydrotalcites: Aluminum source effect on physicochemical properties. *Mater. Lett.* **1997**, *31*, 311–316.
- (30) Lee, J. Y.; et al. Synthesis of hydrotalcite type layered double hydroxide with various Mg/Al ratio and surface charge under controlled reaction condition. *Appl. Clay Sci.* **2016**, *134*, 44–49.
- (31) Jitianu, M.; Gunness, D. C.; Aboagye, D. E.; Zaharescu, M.; Jitianu, A. Nanosized Ni-Al layered double hydroxides-Structural characterization. *Mater. Res. Bull.* **2013**, *48*, 1864–1873.
- (32) Sun, P.; et al. Single-layer nanosheets with exceptionally high and anisotropic hydroxyl ion conductivity. *Sci. Adv.* **2017**, *3*, e1602629–e1602636.
- (33) Radha, A. V.; Kamath, P. V.; Shivakumara, C. Order and disorder among the layered double hydroxides: combined Rietveld and DIFFaX approach. *Acta Crystallogr., Sect. B: Struct. Sci.* **2007**, *63*, 243–250.
- (34) Intissar, M.; Jumas, J. C.; Besse, J. P.; Leroux, F. Reinvestigation of the Layered Double Hydroxide Containing Tetravalent Cations: Unambiguous Response Provided by XAS and Mössbauer Spectroscopies. *Chem. Mater.* **2003**, *15*, 4625–4632.
- (35) Ogawa, M.; Inomata, K. Preparation of Mg/Al layered double hydroxide-oleate intercalation compound by a reconstruction method under hydrothermal condition. *Chem. Lett.* **2005**, *34*, 810–811.
- (36) Kovanda, F.; et al. Effect of hydrothermal treatment on properties of Ni-Al layered double hydroxides and related mixed oxides. *J. Solid State Chem.* **2009**, *182*, 27–36.
- (37) Boumeriame, H.; et al. Layered double hydroxide (LDH)-based materials: A mini-review on strategies to improve the performance for photocatalytic water splitting. *J. Energy Chem.* **2021**, *64*, 406–431.

- (38) Holzwarth, U.; Gibson, N. The Scherrer equation versus the 'Debye-Scherrer equation'. *Nat. Nanotechnol.* **2011**, *6*, 534.
- (39) Muniz, F. T. L.; Miranda, M. A. R.; Morilla dos Santos, C.; Sasaki, J. M. The Scherrer equation and the dynamical theory of X-ray diffraction. *Acta Crystallogr., Sect. A: Found. Adv.* **2016**, *72*, 385–390.
- (40) Ilavsky, J.; et al. Development of combined microstructure and structure characterization facility for in situ and operando studies at the advanced photon source. *J. Appl. Crystallogr.* **2018**, *51*, 867–882.
- (41) Jia, Q.; et al. Precipitation kinetics, microstructure evolution and mechanical behavior of a developed Al-Mn-Sc alloy fabricated by selective laser melting. *Acta Mater.* **2020**, *193*, 239–251.
- (42) Tamaki, T.; Nakanishi, N.; Ohashi, H.; Yamaguchi, T. The effect of particle size and surface area on the ion conductivity of layered double hydroxide. *Electrochem. Commun.* **2012**, *25*, 50–53.
- (43) Lahkale, R.; et al. Nitrate-intercalated $Mg_{1-x}Al_x$ -Layered Double Hydroxides with different layer charges (x): Preparation, characterization, and study by impedance spectroscopy. *Appl. Clay Sci.* **2018**, *158*, 55–64.
- (44) Lozano, R. P.; Rossi, C.; La Iglesia, Á.; Matesanz, E. Zaccagnaite-3R, a new Zn-Al hydrotalcite polytype from El Soplao cave (Cantabria, Spain). *Am. Mineral.* **2012**, *97*, 513–523.
- (45) Sokol, D.; Salak, A. N.; Ferreira, M. G. S.; Beganskiene, A.; Kareiva, A. Bi-substituted Mg_3Al-CO_3 layered double hydroxides. *J. Sol-Gel Sci. Technol.* **2018**, *85*, 221–230.
- (46) Parker, L. M.; Milestone, N. B.; Newman, R. H. The Use of Hydrotalcite as an Anion Absorbent. *Ind. Eng. Chem. Res.* **1995**, *34*, 1196–1202.
- (47) Ahmed, A. A. A.; Talib, Z. A.; Hussein, M. Z. B.; Zakaria, A. Improvement of the crystallinity and photocatalytic property of zinc oxide as calcination product of Zn-Al layered double hydroxide. *J. Alloys Compd.* **2012**, *539*, 154–160.
- (48) Gadikota, G.; Zhang, F.; Allen, A. J. Towards understanding the microstructural and structural changes in natural hierarchical materials for energy recovery: In-operando multi-scale X-ray scattering characterization of Na- and Ca-montmorillonite on heating to 1150 °C. *Fuel* **2017**, *196*, 195–209.
- (49) Fujisawa, T.; Kato, M.; Inoko, Y. Structural characterization of lactate dehydrogenase dissociation under high pressure studied by synchrotron high-pressure small-angle X-ray scattering. *Biochemistry* **1999**, *38*, 6411–6418.
- (50) Jensen, G. V.; et al. Anisotropic Crystal Growth Kinetics of Anatase TiO_2 Nanoparticles Synthesized in a Nonaqueous Medium. *Chem. Mater.* **2010**, *22*, 6044–6055.
- (51) Starukh, G.; Rozovik, O.; Oranska, O. Organo/Zn-Al LDH Nanocomposites for Cationic Dye Removal from Aqueous Media. *Nanoscale Res. Lett.* **2016**, *11*, 228.
- (52) Prakruthi, H. R.; Jai Prakash, B. S.; Bhat, Y. S. Microwave assisted synthesis of glycerol carbonate over LDH catalyst: Activity restoration through rehydration and reconstruction. *J. Mol. Catal. A: Chem.* **2015**, *408*, 214–220.
- (53) Bravo-Suárez, J. J.; Páez-Mozo, E. A.; Oyama, S. T. Review of the synthesis of layered double hydroxides: A thermodynamic approach. *Quim. Nova* **2004**, *27*, 601–604.

NOTE ADDED AFTER ASAP PUBLICATION

Author name Wai Kian Tan was correctly spaced on February 28, 2023.